η = packing fraction in the bulk phase = $\pi c_b d^3 N_A/6$
η_1 = linear packing fraction = $c_1 N_A d$
η_2 = two-dimensional packing fraction = $\pi c_2 d^2 N_A/4$
κ_T = isothermal compressibility
κ_T^* = dimensionless isothermal compressibility = $RT(\partial c_b/\partial p)_T$; group defined by Eq. 28
λ = size ratio = d/D
μ = size ratio = D/d; chemical potential
Ξ = grand-canonical partition function
Π = osmotic pressure
ϕ_1, ϕ_2 = fugacity coefficients for a one- and two-dimensional fluid, respectively

Subscripts

b = bulk phase
o = pure solvent

LITERATURE CITED

Anderson, J. L., and J. A. Quinn, "Restricted Transport in Small Pores," *Biophys. J.*, **14**, 130 (1974).

Barker, J. A., and D. Henderson, "What is Liquid? Understanding the States of Matter," *Rev. Mod. Phys.*, **48**, 587 (1976).

Bellemans A., "Statistical Mechanics of Surface Phenomena," part I, *Physica*, **28**, 493 (1962); part II, *ibid.*, **28**, 617 (1962).

Brenner, H., and L. J. Gaydos, "The Constrained Brownian Movement of Spherical Particles in Cylindrical Pores of Comparable Radius," *J. Colloid Int. Sci.*, **58**, 312 (1977).

Brochard, F., and P. G. de Gennes, "Conformations de Polymeres Fondus dans des Pores Tres Petits," *J. Physique*, **40**, L-399 (1979).

Carnahan, N. F., and K. E. Starling, "Equation of State for Nonattracting Rigid Spheres," *J. Chem. Phys.*, **51**, 635 (1969).

Casassa, E. F., "Equilibrium Distribution of Flexible Polymer Chains between a Macroscopic Solution Phase and Small Voids," *J. Polymer Sci.*, **B5**, 773 (1967).

Casassa, E. F., "Comments on Exclusion of Polymer Chains from Small Pores and Its Relation to Gel Permeation Chromatography," *Macromolecules*, **9**, 182 (1976).

Casassa, E. F., and Y. Tagami, "An Equilibrium Theory for Exclusion Chromatography of Branched and Linear Polymer Chains," *Macromolecules*, **2**, 14 (1969).

Daoud, M., and P. G. de Gennes, "Statistics of Macromolecular Solutions Trapped in Small Pores," *J. Physique*, **38**, 85 (1977).

Fischer, J., "Fourth-Order Interaction of Hard Spheres with a Hard Wall," *Mol. Phys.*, **35**, 897 (1978).

Giddings, J. C., E. Kucera, C. P. Russell, and M. N. Myers, "Statistical Theory for the Equilibrium Distribution of Rigid Molecules in Inert Porous Networks: Exclusion Chromatography," *J. Phys. Chem.*, **72**, 4397 (1968).

Glandt, E. D., "Density Distribution of Hard-Spherical Molecules inside Small Pores of Various Shapes," *J. Colloid Int. Sci.*, **77**, 512 (1980).

Heckmann, K., "Single File Diffusion," *Biomembranes*, K. Kreuzer and J. F. G. Slegers, eds., **3**, Plenum, N.Y., 127 (1972).

Henderson, D., "Monte Carlo and Perturbation Theory Studies of the Equation of State of the Two-Dimensional Lennard-Jones Fluid," *Mol. Phys.*, **34**, 301 (1977).

Kratky, K. W., "Fifth to Tenth Virial Coefficients of a Hard-Sphere Fluid," *Physica*, **87A**, 584 (1977).

McMillan, W. G., and J. E. Mayer, "The Statistical Thermodynamics of Multicomponent Systems," *J. Chem. Phys.*, **13**, 276 (1945).

Pickard, D. K., and E. M. Tory, "The Radial Distribution Function of Hard Rods," *J. Chem. Phys.*, **70**, 5923 (1979).

Salzburg, Z. W., R. W. Zwanzig, and J. G. Kirkwood, "Molecular Distribution Functions in a One-Dimensional Fluid," *J. Chem. Phys.*, **21**, 1098 (1953).

Satterfield, C. N., C. K. Colton, B. de Turckheim, and T. M. Copeland, "Effect of Concentration on Partitioning of Polystyrene within Finely Porous Glass," *AIChE J.*, **24**, 937 (1978).

Steele, W. A., "The Interaction of Gases with Solid Surfaces," Pergamon, Oxford (1974).

Tonks, L., "The Complete Equation of State of One-, Two-, and Three-Dimensional Gases of Hard Elastic Spheres," *Phys. Rev.*, **50**, 955 (1936).

Manuscript received February 12, 1980; revision received April 22, and accepted May 7, 1980.

Gas-Phase Combustion in Fluidized Beds

Kerosine or propane was injected near the base of a small, air-fluidized bed of sand at 940°C. The fraction of fuel burnt within the bed was determined from a heat balance, for various particle sizes, fluidizing velocities, and bed depths.

Assuming the initial formation of a train of fuel vapor bubbles, theoretical analysis indicated two stages of combustion: (1) rapid consumption of the oxygen initially between fuel vapor bubbles; (2) slow consumption of oxygen initially outside the fuel vapor region by radial diffusion of oxygen and fuel vapor, analogous to a diffusion flame.

Comparison of experiment with theory gave effective radial diffusion coefficients of the same order of magnitude as the molecular diffusion coefficient. It was inferred that combustion occurs largely by a diffusion flame within the bed, with diffusion through the particulate phase being the rate-controlling step. This explains why fuel distribution is so important in attaining efficient combustion.

J. F. STUBINGTON

Dept. of Fuel Technology
University of N.S.W.
Sydney, Australia

J. F. DAVIDSON

Dept. of Chemical Engineering
University of Cambridge
Pembroke Street
Cambridge, England

SCOPE

The objective of this work was to elucidate the mechanism of combustion of oil or gas injected at a single point into an air-fluidized bed of inert particles such as sand. Intuition suggests that the high degree of mixing in a violently fluidized bed would facilitate combustion, so that complete combustion would occur within a short distance from the point of injection, provided the fluidizing air supplied was sufficient to burn the fuel.

On the other hand, when oil or gas is injected into an air-fluidized bed, overbed burning may occur unless the number of fuel injection points is adequate, perhaps 1/m^2 of superficial area for a large industrial fluidized combustor. This work

0001-1541-81-4213-0059-$2.00.

indicates the factors governing the spacing of fuel injection points for liquid and non-premixed gaseous fuels. The results may also be applied to the burning of coal containing an appreciable proportion of volatile matter, whose combustion is likely to be governed by the same factors as the combustion of liquid and gaseous fuels.

The experimental program was conducted on a 78-mm diameter by 120-370 mm high, air-fluidized bed of sand at ~ 940°C, with propane or kerosine injection near the base of the bed. The percentage of injected fuel burnt in the bed was determined from a heat balance; the effects of bed height, particle diameter, and fluidizing velocity were studied. Theoretical analysis assumed that the fuel initially forms a train of fuel vapor bubbles and that the rate of combustion is governed by the subsequent diffusion through the bed of fuel vapor and oxygen from the fluidizing air. This theory led to the conclusion that there is a laminar diffusion flame within the particulate phase, where the fluid motion is laminar even in a violently bubbling bed. Comparison of this theory with the experimental data gave a value for the effective radial diffusion coefficient for oxygen and fuel vapor D_e of the same order as the molecular diffusion coefficients.

This theory is tentative. Other rate-controlling steps that may contribute to the overbed burning are as follows.

1. By-passing of fuel bubbles rising through fuel-rich regions without contacting oxygen. This may have been a factor in the present experiments.

2. By-passing of oxygen in large bubbles initially containing air. This may be important in large industrial beds, but order-of-magnitude calculations indicate that it was not a controlling step in the present experiments.

CONCLUSIONS AND SIGNIFICANCE

1. Combustion of non-premixed gaseous and liquid fuels in a fluidized bed depends on diffusion of fuel vapor and oxygen in the particulate phase: this is a relatively slow process because the fluid motion in the particulate phase is laminar, even in a violently bubbling bed.

2. The diffusion-controlled combustion process for a single fuel injection point has been described in two stages: (a) the reaction of fuel with the oxygen between successive fuel bubbles, which occurs within a very small distance above the fuel injection point; and (b) the radial diffusion of fuel and oxygen to a reaction "surface" within the bed, analogous to a diffusion flame.

3. Other possible by-passing mechanisms are: (a) fuel-rich bubbles which may rise through fuel-rich regions of the bed and reach the surface without contacting oxygen; (b) large bubbles which initially containing only air become depleted of oxygen by cross-flow with the particulate phase. These may reach the bed surface with a higher oxygen concentration than the average exit concentration over the whole bed.

It is believed that these two mechanisms may be important for deep beds: when the bed depth is more than 1 m, the mechanism of Figure 4 would not be limiting.

4. The present results may explain some facts well known to designers and operators of fluidized combustors. (a) It is known that gas can be burnt in a very shallow fluidized bed (e.g., 100 mm), if the gas is premixed with air before entering the bed. (b) For oil combustion, it is known that many injection nozzles are required (e.g., 1/m^2 bed area) and the same is true for the combustion of coal containing a high proportion of volatile matter, whose combustion would be governed by the process described here.

EXPERIMENTS

Heat Balance

The essence of the experiment was to use a heat balance to deduce the percentage of fuel burnt in a fluidized bed. The fuel (liquid or gaseous) was injected through a single orifice just above the distributor of an air-fluidized bed of sand. Due to incomplete mixing between fuel and oxygen in the bed, a proportion of the fuel escaped unburnt from the top of the bed: a flickering diffusion flame could sometimes be seen just above the bed surface.

The apparatus is shown diagrammatically in Figure 1. The bed of sand was contained in a 78-mm I. D. quartz tube, 600 mm high with a stainless steel woven mesh distributor. To eliminate temperature gradients within the bed at low fluidizing velocities, the inlet air was preheated in a stainless steel tube, of the same diameter as the bed, immediately below the distributor (Figure 1). The heat loss from the bed was reduced by electrical heating of Kanthal resistance wire wound around the quartz tube, so that power could be supplied to the bottom third, two-thirds, or the whole heater, Figure 1.

The bed was insulated with Kaowool to minimize the heat loss, which was estimated from the readings of the two "heat-loss" thermocouples (2 and 3 of Figure 1). These were embedded in the insulation at the same height, but at different radii, and the difference between the readings indicated the temperature gradient through the insulation. The air temperature just below the distributor was measured by thermocouple 1. The bed temperature was an average of those thermocouples which were immersed in the bed (4, sometimes 5, and occasionally 6 depending on bed height). The gases leaving the bed were assumed to be at bed temperature. The unburnt fuel leaving the bed often caused a flickering flame in the freeboard, but the overbed temperature rise could not be used to deduce the amount of unburnt fuel leaving the bed because of: (i) the well-known difficulty of measuring flame temperatures, (ii) the heat losses through the wall of the freeboard and by radiation, and (iii) the possibility of mixing at the exit with ambient air.

When combustion generates heat at the rate P_C, a heat balance on the bed gives:

$$P_I + P_E + P_C = P_O + P_L \tag{1}$$

where P_I and P_O represent the convective heat flows of the inlet and outlet gas streams respectively, and P_E is the power supplied to the main heater. The rate of heat loss P_L was estimated from a blank experiment with no fuel supplied, but with the same fluidizing velocity as the combustion experiment. The electrical power supplies were adjusted to give: (1) the same temperature difference between the two heat-loss thermocouples (i.e., the same rate of heat loss through the insulation); and (2) the same inlet air temperature below the distributor. Then,

$$P_L = P_I' - P_O' + P_E' \tag{2}$$

where the dashes denote the blank experiment.

Eliminating P_L from Eqs. 1 and 2 gives:

$$P_C = (P_E' - P_E) + (P_O - P_O') - (P_I - P_I') \tag{3}$$

which was used to calculate the rate of heat generation within the bed by combustion.

Fuel Injection

Liquid kerosine or propane gas was supplied to the fuel injection tube through separate rotameters. To prevent blockage of the tube by sand, the injection orifice faced horizontally rather than vertically upward, Figure 1. With propane injection, cracking was negligible, but with kerosine injection, a carbon deposit built up in the tube. This problem was solved by surrounding the injection tube with a larger concentric tube and passing cooling air through the annulus between the tubes. With this arrangement, the kerosine was partially vaporized before entering the bed.

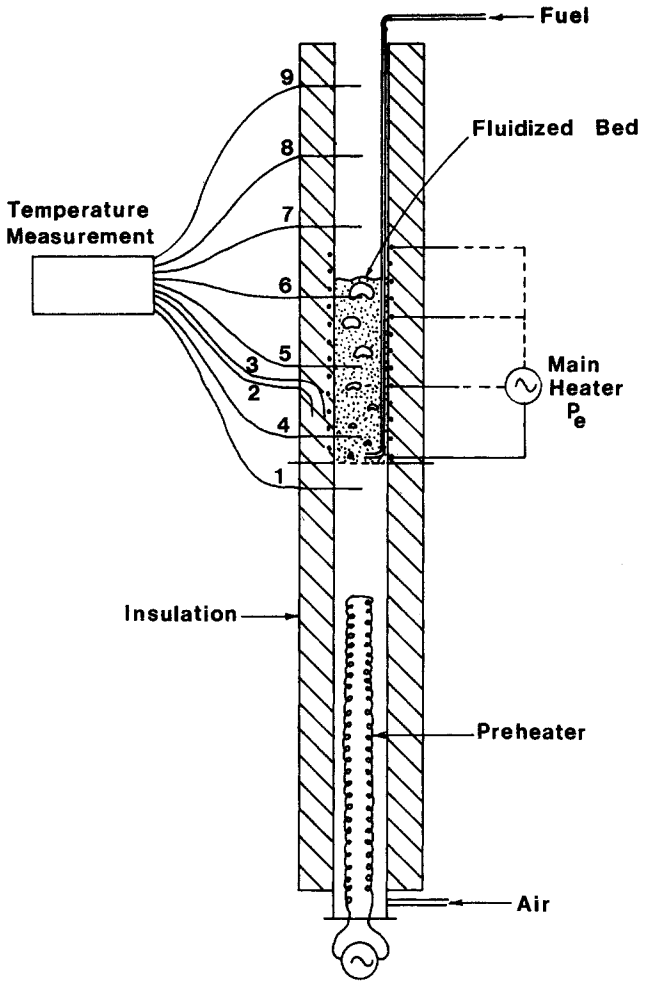

Figure 1. Apparatus for measuring the percentage fuel burnt in an air-fluidized bed of sand, for single point injection of propane or kerosine.

For propane injection through a single tube, a small capacitance probe was used to measure the frequency of bubble formation at the orifice, using the method of Harrison and Leung (1961). With a propane flowrate between 8 and 24 cc/s at 20°C, the bubble frequency varied from 13 to 15 Hz (Stubington, 1973). At the bed temperature of 940°C, the volumetric flowrate ranged from 33 to 99 cc/s and the corresponding theoretical frequency (Davidson and Harrison, 1963) is from 27 to 22 Hz, somewhat higher than observed but of the same order of magnitude. It was concluded that propane forms regular bubbles by a mechanism similar to that of a nonreacting gas blown into a fluidized bed.

For kerosine injection, the bubbling was too irregular to measure using the capacitance technique, presumably due to the vaporization of some kerosine in the injection tube. It was therefore assumed that, for a given volumetric flow rate of fully vaporized kerosine, the bubble frequency was the same as for propane.

Incipient Fluidizing Velocities

The caption to Figure 5 shows the size range of each charge of sand particles, determined by sieving. The solid density was 2,580 kg/m^3. For the two larger particle sizes, the incipient fluidizing velocity U_{mf} was determined from the intersection of two straight lines on a plot of bed pressure drop against fluidizing velocity at the bed temperature of 940°C. Each point on this plot was obtained by decreasing the fluidizing velocity from well above U_{mf} to maintain a uniform bed temperature prior to taking the measurements. Assuming that the relation between U_{mf} and particle diameter d_p follows the correlation of Kunii and Levenspiel (1969); this correlation was then used to estimate a mean particle diameter for each of the two largest particle size ranges. These estimated values agreed well with the arithmetic mean of the maximum and minimum screen sizes in Figure 5. Values of U_{mf} were therefore calculated from the correlation of Kunii and Levenspiel (1969), using this arithmetic mean as the effective d_p.

Maximum Bed Height

The maximum bed height was measured by direct observation of the injection tube while lowering it into the bed. This height was taken to be the position of the injection orifice when the horizontal part of the injection tube was just covered by particles as the largest slug broke through the surface. Because of the fluctuating nature of the slugging, the measured bed heights were not particularly accurate at higher fluidizing velocities.

THEORY

Cloudless and Clouded Fuel Bubbles

The fuel is injected into an air-fluidized bed from a point source and it will be assumed that the fuel, whether initially liquid or gaseous, forms regular vapor bubbles as indicated in Figure 2. Because of the cross-flow between bubble and particulate phases, the fuel will be swept out of each bubble into the particulate phase, and two cases must be considered:

(1) For large particles, $u_{mf} > u_b$. In this case, the fluidizing gas streamlines from the bubble extend continuously up into the particulate phase, but there is a limiting radius a shown in Figure 2(a), reached by a streamline starting from the edge of a bubble.

(2) For small particles, $u_{mf} < u_b$ and a "cloud" is formed. The vapor within the bubble only penetrates a finite distance into the particulate phase, Figure 2(b).

Kunii and Levenspiel (1969) distinguish between these cases by the terms "slow" and "fast" bubbles, which imply a change in bubble velocity with changing particle diameter. Actually, the bubble velocity is independent of particle size and it is the interstitial fluidizing velocity that changes between the two cases. Hence, the terms slow and fast are inappropriate when applied to the bubble. We prefer to distinguish between cases (1) and (2) by using the terms "cloudless" bubble for (1) and "clouded" bubble for (2).

With cloudless bubbles, the fuel is swept out into the particulate phase above the bubble by the cross-flow. The streamlines

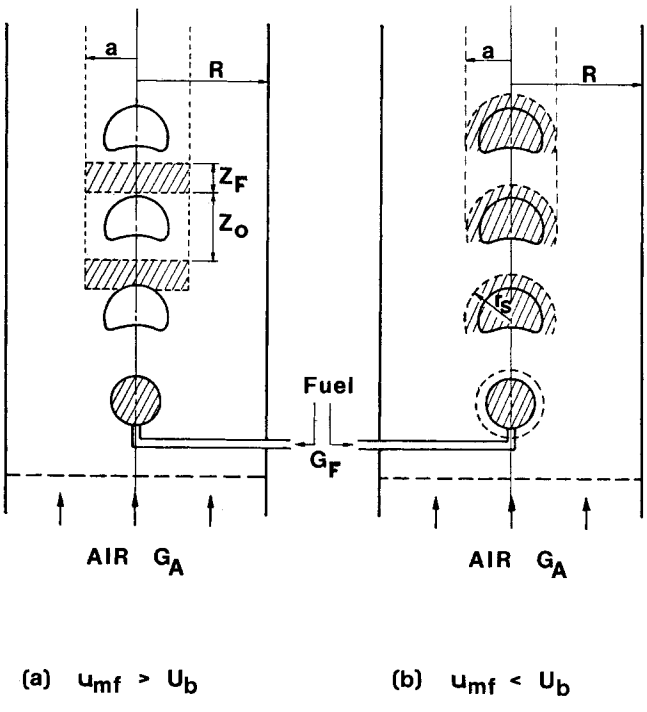

Figure 2. Initial distribution of fuel injected into a fluidized bed for (a) cloudless fuel bubbles; and (b) clouded fuel bubbles. Fuel rich regions are shaded, and a is the radius of the region containing fuel at the conclusion of stage 1 combustion.

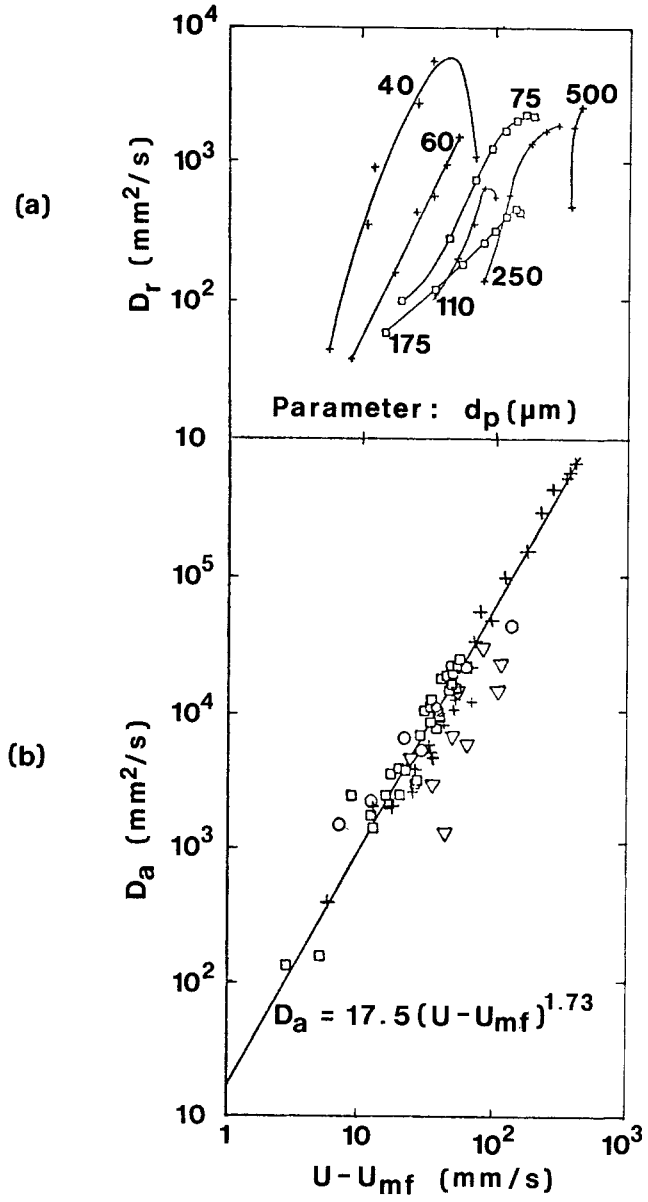

Figure 3. Dispersion coefficients in fluidized beds, resulting from large-scale mixing processes: (a) axial, D_a; and (b) radial, D_r.
- ○ Baerns
- □ Baerns, Fetting, and Schügerl
- ▽ Latham, and Potter
- \+ Schügerl

converge as the flow enters the bubble from below and diverge as the vapor leaves the bubble at the top. Assuming plug flow within the bubble, the fuel vapor is swept upwards into the particulate phase, to give bands of fuel-rich regions between bubbles as indicated in Figure 2(a).

With a clouded bubble, the oxygen within the cloud is usually much less than the stoichiometric requirement for the fuel that initially forms the bubble. This oxygen reacts with fuel from the bubble, and the cloud and bubble within it soon become a region containing only fuel, nitrogen, and combustion products. Subsequently, the fuel can burn only at the cloud boundary, where there must be a diffusion flame. Figure 2(b) shows the situation with a succession of clouded bubbles forming at the fuel injection orifice.

Combustion by Mixing of Fuel and Oxygen

The fuel vapor, initially distributed as shown in Figure 2, cannot burn until it mixes with oxygen (the temperature being sufficient for reaction rates to be rapid) and the rate of combustion is determined by the rate of mixing. Therefore, literature data on radial and axial dispersion coefficients, D_r and D_a, were correlated, Figure 3. These values of D_r and D_a were determined by tracer gas injection in small diameter beds. The dependence of D_a on excess gas velocity ($U - U_{mf}$) shows that bubbling is the factor controlling axial dispersion of injected tracer gas. The values of D_a are much greater than D_r because of: (i) transport of gas due to bubbles, and (ii) circulation currents.

Stage 1 Combustion

Stage 1 is the consumption of oxygen within the radius "a" of Figure 2 (i.e., oxygen initially between fuel vapor bubbles). Radius a is determined by the streamlines from the side of the bubble for a cloudless bubble, and by the cloud radius for a clouded bubble, the method of calculation being described in Appendix 1.

For the diffusion of fuel and oxygen in this region, radial dispersion was assumed negligible in comparison with axial dispersion since $D_a >> D_r$. Results of the theory show that the oxygen is all used up within about 1 mm above the fuel injection point (Stubington, 1973).

The use of D_a to calculate the diffusion of fuel and oxygen in stage 1 is to some extent inconsistent with the results of the stage 2 analysis (see below), since the experimentally determined

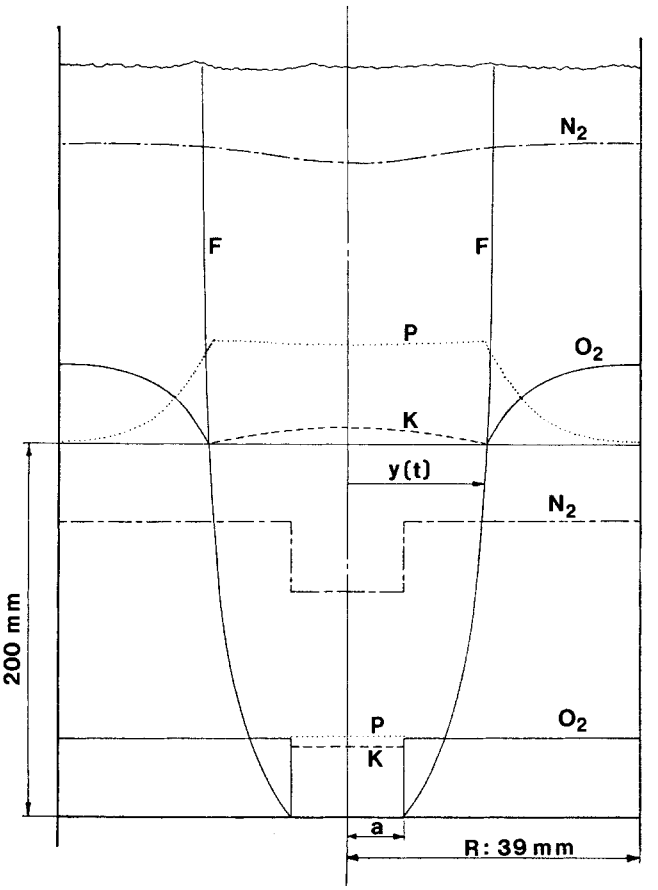

Figure 4. Stage 2 combustion governed by radial diffusion of kerosine K and oxygen O_2. Product (P) and nitrogen (N_2) concentrations are also shown. The flame front (F) and concentration profiles at height 200 mm are to scale with D_r = 160 mm²/s.

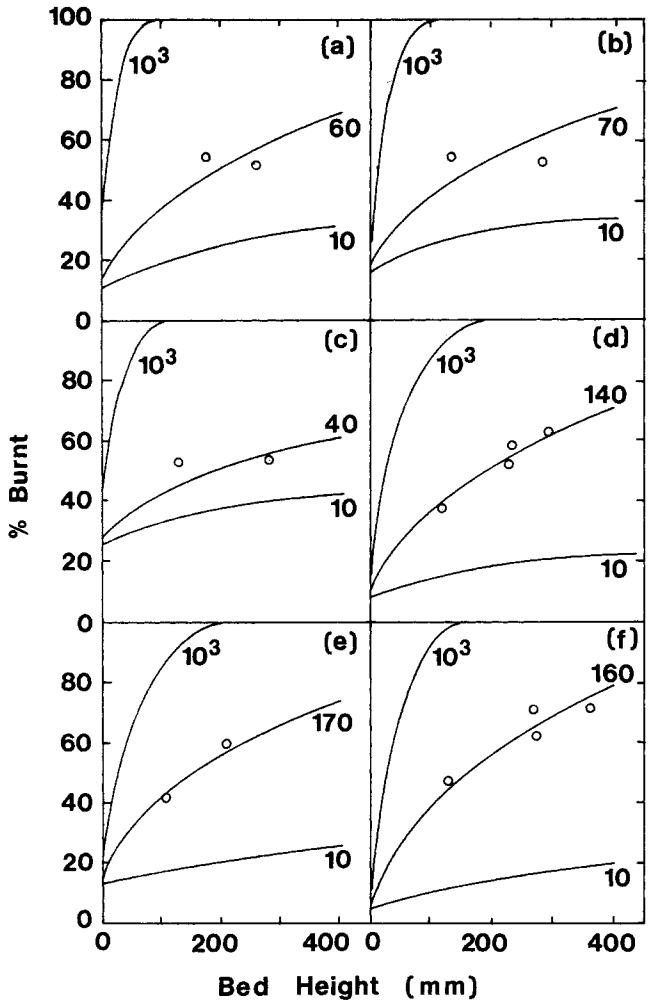

Figure 5. Experimental results ○ compared with theoretical curves using different values of effective radial diffusion coefficient D_e (mm²/s) shown as parameter.

Figure	Size range (μm)	Estimated diameter (μm)	U_{mf} (mm/s at 940°C)	$U - U_{mf}$ (mm/s)	Fuel
a	106-125	115	4	355	Propane
b	300-350	325	35	355	Propane
c	420-500	460	70	355	Propane
d	600-850	750	185	355	Propane
e	850-1000	913	274	355	Propane
f	600-850	750	185	260	Kerosine

effective radial diffusivity was of the same order of magnitude as the molecular diffusion coefficient (i.e., much less than D_a). However, even if the molecular diffusion coefficient were used in place of D_a for the stage 1 calculations, this stage would still be complete within a smaller height than is required for stage 2. Hence, the overall rate of combustion will still be controlled by the rate of the stage 2 processes.

Stage 2 Combustion

The second stage of combustion is concerned with reaction between fuel vapor contained in the roughly cylindrical core (of initial radius "a") and oxygen from the air in the surrounding annulus. Radial diffusion of fuel vapor and oxygen to the reaction zone between these regions controls the rate of combustion. The analysis is similar to that of Burke and Schumann (1928) for a diffusion flame, and the equations are given in Appendix 2. Figure 4 shows the resulting concentration profiles for a typical case assuming an effective radial diffusion coefficient D_e of 160 mm²/s. Initially, it was thought that values of D_r from Figure 3(b) would be relevant. However, these values gave more complete combustion than was observed experimentally, and it was concluded that a slower diffusion process must occur. Therefore, values of the effective radial diffusion coefficient were inferred to fit the observed degree of combustion.

The analysis of Burke and Schumann neglects axial diffusion and is valid only for tall flames. This analysis would not apply if the values of D_a and D_r from Figure 3 were relevant. However, the experimental results indicate a much slower diffusion process, and this implies a tall flame to which the Burke and Schumann analysis does apply.

Some backmixing of gas would be expected for the finest particles, decreasing as the particle size increased. Backmixing has not been considered in the model because it is a large-scale mixing process acting mainly in the axial direction. It is not expected to contribute significantly to radial mixing on a molecular scale, which controls the stage 2 combustion.

Although the theory was based on the supposition of an inner zone containing fuel and no oxygen and a surrounding zone containing oxygen and no fuel, with a roughly cylindrical interface between these zones, it is clear that the interface would intersect bubbles within the bed. (These were large enough to be termed slugs at the top of the deeper beds used.) Calculation of the Reynolds No. for flow through a bubble gave maximum values ranging from 5 to 320, indicating laminar flow through the bubble as well as through the particulate phase. Two possible effects of these bubbles on stage 2 combustion are noted:

(1) Because of the compression of the streamlines as they pass through a bubble, the shape of the interface will be distorted from that shown in Figure 4 in the neighborhood of a bubble.

(2) Coalescence of those bubbles through which the interface passes may cause some additional radial mixing of fuel and oxygen by disturbing the laminar flow of gases through the bubble. (Coalescence of bubbles wholly within the oxygen zone or the fuel zone would not affect the radial mixing process or enhance the rate of stage 2 combustion).

Since the interface would intersect some bubbles, both of the above processes may increase the rate of combustion. However, the picture given by Figure 4 is believed to represent generally the state of affairs in the bed, and especially the state of affairs in the particulate phase.

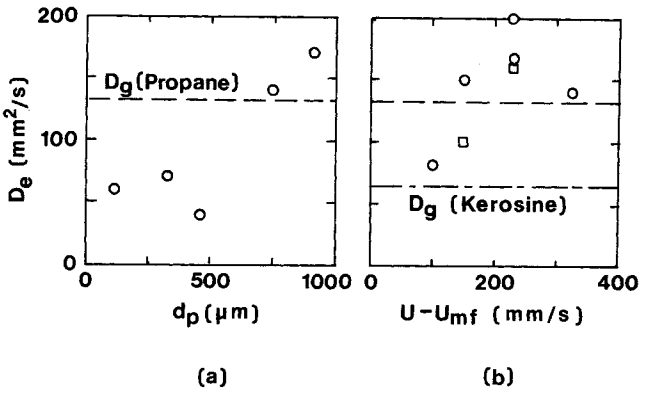

Figure 6. Effective radial diffusion coefficients, D_e.
(a) Effect of particle diameter ($U - U_{mf}$ = 355 mm²/s and excess air = 50%.)
(b) Effect of fluidizing velocity (d_p = 750 μm). Experimental results: propane ○, kerosine □. D_g is the molecular diffusion coefficient in air at 940°C.

Transfer of Oxygen from Bubbles to Particulate Phase

The above analysis is based on the assumption that the rate controlling process is diffusion of oxygen and fuel vapor towards a flame front within the particulate phase. This presupposes an adequate supply of oxygen in the particulate phase. Order of magnitude calculations show that there is adequate transfer of oxygen from bubbles to particulate phase. For these calculations, $(U - U_{mf}) = 0.35$ m/s, $H_{mf} = 0.3$ m, $D_g = 200$ mm^2/s, and the bubble size was calculated from the correlation of Darton et al. (1977) giving $d_e = 0.06$ m. The number of times the bubble is swept out on passing through the bed X was calculated (Davidson and Harrison, 1963) and ranged from 3 to 14 for the particle sizes used in the present experiments (U_{mf} from 0.004 to 0.274 m/s). With such large values of X, there is very effective transfer of oxygen from bubbles to particulate phase.

For a large bed, the bubble diameter could be much greater, giving a smaller value of X, so that the interphase transfer of oxygen from bubble to particulate phase would be controlling. Overbed burning might then occur, not due to diffusion control as in the present case, but due to interphase transfer being a controlling factor.

RESULTS AND COMPARISON WITH THEORY

Figure 5 shows some experimental measurements of the percentage of fuel burnt in the bed as a function of bed height for a variety of conditions. The curves were calculated from the above theory: in each case three values of the radial diffusion coefficient D_e were used, and the value of D_e giving the best fit to the data was inferred. Note that each curve intercepts the ordinate at a finite % burnt: this is the consumption during stage 1 combustion. As already described, the height required to complete stage 1 combustion is negligible compared with the height for stage 2 combustion, which thus dominates Figure 5.

The values of D_e inferred from Figure 5 are quite modest, of the same order as the relevant molecular diffusion coefficients at the bed temperature, which are:

(i) kerosine vapor in air—64 mm^2/s,
(ii) propane in air—132 mm^2/s, and
(iii) oxygen in air—240 mm^2/s.

The inferred values of D_e, 40-170 mm^2/s, are considerably less than the values of D_r shown in Figure 3(a), which are in the range 100-10,000 mm^2/s.

The low values of D_e obtained from our experiments may occur because the ultimate mixing between fuel and oxygen is by molecular diffusion in the particulate phase and in those bubbles which lie on the interface between fuel and oxygen regions. Although the bed was bubbling violently or even slugging, the particle Reynolds No. is of the order of unity, indicating laminar flow in the particulate phase. In contrast, measurements of D_r by time-averaged concentration profiles of an injected tracer gas would be enhanced by bubbling. Whereas combustion requires mixing on a molecular scale, the dispersion of tracer gases is determined by large-scale mixing processes and the value of D_r does *not* indicate the rate of molecular mixing.

Some support for this picture is provided by Figure 6, which shows: D_e as a function of particle diameter for $U - U_{mf} = 355$ mm/s; and D_e as a function of $U - U_{mf}$ for the larger particles $d_p = 750$ μm. Figure 6(a) suggests that D_e increases with particle diameter which is consistent with diffusion through the particulate phase. On the other hand, Figure 6(b) shows an increase in D_e with $(U - U_{mf})$, suggesting that the bubbling does influence the rates of mixing of fuel and oxygen. This may be explained by the distortion of the fuel/oxygen interface in the neighborhood of bubbles and the coalescence of bubbles intersected by the interface, as described previously.

Günther (1971) obtained similar results from an 800-mm I.D. combustor. He injected towns gas at the middle of an air fluidized bed and determined the "mean degree of combustion" as a function of bed height. Radial dispersion coefficients D_r were determined by tracer experiments on a cold model of the combustor, but the results were markedly different from the combustion data.

Two further points should be made in considering our results:

(i) The high values of D_a used to estimate the rate of stage 1 combustion may not be justified. Since the bubbles have little influence on stage 2 combustion, they may be similarly ineffective during stage 1. However, even if D_a were replaced by D_e for the stage 1 calculations, the height required for stage 1 (to burn all the oxygen between successive fuel bubbles) would be less than that for stage 2, because the fuel bubbles are rather close together.

(ii) Some of the fuel by-passing may be due to fuel-rich bubbles passing through the fuel-rich zone, increasing the mean velocity of fuel vapor in this zone above the bed average velocity. Observation of the flame above the bed supported this postulate, since the flame was occasionally augmented by a 'pop' of fuel breaking through the bed surface.

APPENDIX 1: EVALUATION OF a

We assume that the fuel vapor forms regular bubbles whose volume V is determined from $V = G_F/f$, *where* G_F is the volumetric fuel vapor flowrate at the bed temperature and f is the experimentally measured bubble frequency. These bubbles are cloudless or clouded depending on the relative magnitudes of u_{mf} and u_b, the bubble rise velocity.

Cloudless Bubbles

Figure 2(a) illustrates this regime. We assume that the fuel is swept out into the particulate phase by the cross-flow Q, which is calculated by the method of Davidson and Harrison (1963). From each bubble, fuel vapor is supplied to the bed during a period V/Q; and during this time, the first fuel vapor to enter the particulate phase will have risen a height $UV/Q\epsilon$, since the mean upward velocity in the whole bed is U/ϵ. Hence, the height of the fuel vapor region in the bed immediately after all the fuel is flushed out of the bubble will be $Z_F = UV/Q\epsilon$, as shown in Figure 2(a). These regions containing fuel are separated by regions containing oxygen but no fuel, and the periodicity of the phenomenon leads to the relation, $Z_F + Z_O = U/\epsilon f$, from which Z_O may be determined.

In stage 1, the oxygen in the height Z_O is burnt with some of the fuel in the height Z_F, and the resulting combustion products and unburnt fuel enter the area πa^2, *where* a is indicated in Figure 2(a). The value of a is calculated by assuming uniform velocity across the bed, and determining the ratio of the volumetric flows into the whole bed (of radius R) and into the area πa^2. The volumetric flow rate of air entering the area πa^2 is $Z_O G_F/Z_F$, so the flow of air plus fuel into that area is $(1 + Z_O/Z_F)G_F$. The volumetric air flowrate to the whole bed is G_A so the total volumetric flowrate to the whole bed is $G_A + G_F$. For cloudless bubbles, a is calculated from:

$$R^2/a^2 = (G_A + G_F)/[G_F(1 + Z_O/Z_F)]$$

Clouded Bubbles

When $u_{mf} < u_b$, a "cloud" is formed, Figure 2(b). The cloud radius r_s is calculated from the analysis by Davidson and Harrison (1963). It is assumed that all of the oxygen within a cylinder of radius r_s is consumed during stage 1 combustion, leaving an oxygen-free region of radius $a = r_s$ for the start of stage 2 combustion.

APPENDIX 2: RADIAL DIFFUSION-CONTROLLED COMBUSTION

The analysis used is similar to that of Burke and Schumann (1928), but the equations are set out here for completeness. The lower part of Figure 4 shows the concentration profiles at the end of stage 1, when all of the oxygen in the central fuel-rich zone has been consumed. Subsequently, stage 2 combustion occurs by radial diffusion of fuel, oxygen, combustion products, and nitrogen. Since the nitrogen concentration is relatively

high, the other components may be considered to have dilute concentration, and the governing equations for oxygen and fuel are:

$$\frac{\partial C}{\partial t} = \frac{D_e}{r}\frac{\partial}{\partial r}\left(r\frac{\partial C}{\partial r}\right) \tag{A1}$$

where $C = C_F$ for $0 < r \leq y(t)$ in the fuel region, and $C = C_O$ for $y(t) < r < R$ in the oxygen region. R is the radius of the bed and $y(t)$ is the radius of the flame front, Figure 4. The boundary conditions are $\partial C_F/\partial r = 0$ at $r = 0$, $C_F = C_O = 0$ at $r = y(t)$, $\partial C_O/\partial r = -s\,\partial C_F/\partial r$ at $r = y(t)$, and $\partial C_O/\partial r = 0$ at $r = R$; s being the stoichiometric ratio of the number of moles of oxygen required to burn 1 mol of fuel. At $t = 0$, the concentrations are obtained from conditions at the end of stage 1, and are assumed to be uniform throughout the fuel region ($C_F = C_{Fi}$) and throughout the oxygen region ($C_O = C_{Oi}$). Following Burke and Schumann (1928), the two equations (A1) for oxygen and fuel are combined into a single equation by writing $A = sC_F/C_{Oi} - C_O/C_{Oi}$, giving the dimensionless differential equation:

$$\frac{\partial A}{\partial \theta} = \frac{\partial^2 A}{\partial \eta^2} + \frac{1}{\eta}\frac{\partial A}{\partial \eta} \tag{A2}$$

for $0 < \eta < \eta_R$. The dimensionless quantities are $\eta = r/a$, $\eta_R = R/a$, and $\theta = tD_e/a^2$; the boundary conditions become $\partial A/\partial \eta = 0$ at $\eta = 0$ and $\eta = \eta_R$; and the initial conditions become $A = sC_{Fi}/C_{Oi}$ for $0 < \eta < 1$, and $A = -1$ for $1 < \eta < \eta_R$. Eq. A2 has been solved (Stubington, 1973) in terms of Bessel functions, and the solution used to determine concentration profiles for fuel and oxygen as well as the dimensionless radial co-ordinate $y(t)/a$ for the flame front. These results in terms of time t were converted to distance Z above the injector using $Z = Ut/\epsilon$, *where* U is the superficial velocity of gases flowing through the bed and ϵ is the average bed voidage (determined from maximum expanded bed height).

The results of one such calculation are shown in Figure 4, where the flame front is plotted as a function of height above the injection point, and the concentration profiles are shown at the start of stage 2 combustion and at a height of 200 mm above the injector.

ACKNOWLEDGMENT

J. F. Stubington gratefully acknowledges the Royal Commission for the Exhibition of 1851 and Christ's College, Cambridge, for their financial assistance during the course of this work.

NOTATION

a = Radius of the region containing fuel at the end of stage 1 combustion
A = $sC_F/C_{Oi} - C_O/C_{Oi}$
C = concentration of oxygen or fuel
C_F = concentration of fuel
C_{Fi} = initial fuel concentration
C_O = concentration of oxygen
C_{Oi} = initial oxygen concentration
d_e = equivalent bubble diameter
d_p = mean particle diameter
D_a = axial dispersion coefficient for injected tracer gas
D_e = effective radial diffusion coefficient for combustion
D_g = molecular diffusion coefficient
D_r = radial dispersion coefficient for injected tracer gas
f = frequency of bubble formation at fuel injection orifice
G_A = volumetric flow rate of air into fluidized bed (at bed temperature)
G_F = volumetric flow rate of fuel through injection orifice (at bed temperature)
H_{mf} = bed height at minimum fluidizing velocity
P_C = rate of heat release from combustion in bed
P_E, P'_E = rates of electrical power input, for combustion experiment and blank experiment
P_I, P'_I = rates of heat input from fluidizing air, for combustion experiment and blank experiment
P_L = rate of heat loss from bed
P_O, P'_O = rates of heat loss in exhaust gas stream, for combustion experiment and blank experiment
Q = rate of exchange of gas between bubble and particulate phase
r = radial co-ordinate
r_s = radius of penetration sphere around "clouded" bubble
R = radius of combustor
s = stoichiometric ratio of oxygen to fuel
t = time
u_b = bubble rising velocity
u_{mf} = interstitial minimum fluidizing velocity
U = superficial fluidizing velocity
U_{mf} = superficial minimum fluidizing velocity
V = bubble volume
X = number of times the bubble is swept out on passing through the bed
$y(t)$ = radial co-ordinate of flame front
Z = height above injection point
Z_F = initial height of fuel vapor region from a fuel vapor bubble
Z_O = initial height of oxygen region between fuel vapor regions
ϵ = mean bed voidage
θ = tD_e/a^2
η = r/a
η_R = R/a

LITERATURE CITED

Bearns, M., "Fluidization of Fine Particles," *Proceedings of International Symposium on Fluidization*, Eindhoven, 403 (1967).

Bearns, M., F. Fetting, and K. Schügerl, "Radiale und Axiale Gasvermischung in Wirbelschichten," *Chem. Ing. Tech.*, **35**, 609 (1963).

Burke, S. P., and T. E. W. Schumann, "Diffusion Flames," *Ind. Eng. Chem.*, **20**, 998 (1928).

Darton, R. C., R. D. La Nauze, J. F. Davidson, and D. Harrison, "Bubble Growth Due to Coalescence in Fluidised Beds," *Trans. Inst. Chem. Eng.*, London, **55**, 274 (1977).

Davidson, J. F., and D. Harrison, *Fluidised Particles*, Cambridge Univ. Press (1963).

Günther, R., *Verfahrenstechnik*, **5**, No. 3 (1971).

Harrison, D., and L. S. Leung, "Bubble Formation at an Orifice in a Fluidised Bed," *Trans. Inst. Chem. Eng.*, London, **39**, 409 (1961).

Kunii, D., and O. Levenspiel, *Fluidization Engineering*, John Wiley and Sons, New York (1969).

Latham, R., and O. Potter, "Back-Mixing of Gas in a 6-in. Diameter Fluidised Bed," *Chem. Eng. J.*, **1**, 152 (1970).

Schügerl, K., "Experimental Comparison of Mixing Processes in Two- and Three-Phase Fluidized Beds," *Proceedings of International Symposium on Fluidization*, Eindhoven, 782 (1967).

Stubington, J. F., "The Combustion of Oil in Fluidized Beds," Ph.D. Thesis, Cambridge Univ. (1973).

Manuscript received October 1, 1979; revision received April 10, and accepted May 5, 1980.